# Aligned fractures modeled as boundary conditions within saturated porous media and induced anisotropy. A finite element approach.

*Juan E. Santos *, Instituto del Gas y del Petróleo, Facultad Ingeniería, Universidad de Buenos Aires, CONICET, Department of Mathematics, Purdue University and Universidad Nacional de La Plata, Robiel Martínez Corredor, Facultad de Ingeniería, Universidad Nacional de La Plata and José M. Carcione, Istituto Nazionale di Oceanografia e di Geofisica Sperimentale, OGS.*

## SUMMARY

Fractures in a fluid-saturated poroelastic -Biot- medium are very thin, compliant and highly permeable layers. Fracture apertures in reservoir rocks are on the order of millimeters, much smaller that the wavelengths of the predominant travelling waves. Thus, any finite element (FE) procedure would require extremely fine meshes to represent fractures. In this work aligned fractures within a Biot medium are modeled using boundary conditions imposing continuity of the total stress components, pressure discontinuities proportional to average fluid velocities and displacement discontinuities proportional to stress components and average fluid pressures. Besides, a Biot medium with a dense set of aligned fractures behaves as an effective transversely isotropic and viscoelastic (TIV) medium at the macroscale when the predominant wavelengths are much larger than the average distance between fractures. In this work a set of time-harmonic FE experiments are used to determine the stiffness coefficients of TIV medium equivalent to a horizontally fractured Biot medium. The methodology is first validated against a theory valid for flow perpendicular to the fracture layering and then applied in the case of patchy $CO_2$-brine saturation for which no analytical solutions are available.

## INTRODUCTION

Fractured hydrocarbon reservoirs are a subject of interest in exploration and production geophysics, since generally, natural fractures control the permeability of the reservoir (Gurevich, B. et al., 2009). In many cases reservoir rocks contain dense sets of fractures aligned in preferred directions (Gurevich, B., 2003).

Fractures embedded in a fluid-saturated poroelastic medium are very thin compliant and highly permeable layers, with thickness much smaller than the predominant wavelengths of the seismic travelling waves. Thus any FE discretization of a fractured reservoir would require extremely fine meshes to represent fractures and instead a proper set of boundary conditions to model fractures is required.

Here fractures in a Biot medium are modeled using the boundary conditions derived by Nakawa, S. and Schoenberg, M. A. (2007), which impose continuity of the total stress, pressure discontinuities proportional to average fluid velocities and displacement discontinuities proportional to stress components and average fluid pressures. This approach allows to include mesoscopic attenuation and dispersion effects suffered by seismic waves travelling across fractured hydrocarbon reservoirs.

A Biot medium with a dense set of horizontal fractures behaves as a TIV medium for average fracture distances much smaller than the predominant wavelengths of the traveling waves. To determine a long-wave equivalent TIV medium to a horizontally fractured Biot medium we employ a set of harmonic FE compressibility and shear experiments. The FE results are first validated against a theory derived by Krzikalla, F. and Müller, T. (2011) and then applied to a patchy gas-brine saturated fractured sample for which no analytical solutions are available.

## A FRACTURED BIOT MEDIUM AND THE EQUIVALENT TIV MEDIUM

We consider a fractured isotropic Biot medium and let $\mathbf{u}_s$ and $\tilde{\mathbf{u}}_f$, denote the averaged displacement vectors of the solid and fluid phases, respectively. Let $\mathbf{u}_f = \phi(\tilde{\mathbf{u}}_f - \mathbf{u}_s)$ be the relative fluid displacement, where $\phi$ denotes the porosity and set $\mathbf{u} = (\mathbf{u}_s, \mathbf{u}_f)$. Let $\varepsilon(\mathbf{u}_s)$, $\tau(\mathbf{u})$ and $p_f(\mathbf{u})$ denote the strain tensor of the solid, the stress tensor of the bulk material and the fluid pressure, respectively. The stress-strain relations in a Biot medium can be written in the form (Biot, M.A., 1962):

$$\tau_{st}(\mathbf{u}) = 2G\,\varepsilon_{st}(\mathbf{u}_s) + \delta_{st}(\lambda_U \nabla\cdot\mathbf{u}_s + \alpha\, M \nabla\cdot\mathbf{u}_f), \quad (1)$$

$$p_f(\mathbf{u}) = -\alpha\, M \nabla\cdot\mathbf{u}_s - M^{(\theta)}\nabla\cdot\mathbf{u}_f. \quad (2)$$

The coefficient $G$ is equal to the shear modulus of the bulk material, considered to be equal to the shear modulus of the dry matrix. The other coefficients in (1))-(2) can be obtained in terms of $K_s, K_m$ and $K_f$, the bulk moduli of the solid grains, dry matrix and saturant fluid, respectively, (Carcione, 2007). Biot's equations in the diffusive range and in the absence of external forces are (Biot, M.A., 1962):

$$\nabla\cdot\tau(\mathbf{u}) = 0, \quad (3)$$

$$\mathrm{i}\omega\mathbf{u}_f + \frac{\mu}{\kappa}\nabla p_f(\mathbf{u}) = 0, \quad (4)$$

where $\mathrm{i} = \sqrt{-1}$, $\omega$ is the angular frequency, $\mu$ is the fluid viscosity and $\kappa$ is the frame permeability.

## BOUNDARY CONDITIONS AT FRACTURES AND THE EQUIVALENT TIV MEDIUM

Consider a rectangular domain $\Omega = (0, L_1)\times(0, L_3)$ with boundary $\Gamma$ in the $(x_1, x_3)$-plane, with $x_1$ and $x_3$ being the horizontal and vertical coordinates, respectively. Assume a Biot medium $\Omega$ with a set of $J^{(f)}$ horizontal fractures $\Gamma^{(f,l)}, l = 1, \cdots, J^{(f)}$, each one of length $L_1$ and aperture $h$. This set of fractures divides $\Omega$ in nonoverlapping rectangles $R^{(l)}$, so that $\Omega = \cup_{l=1}^{J^{(f)}+1} R^{(l)}$.

Consider a fracture $\Gamma^{(f,l)}$ and the two rectangles $R^{(l)}$ and $R^{(l+1)}$ having as a common side $\Gamma^{(f,l)}$. Let $\nu_{l,l+1}$ and $\chi_{l,l+1}$ be the unit outer normal and a unit tangent (oriented counterclockwise) on $\Gamma^{(f,l)}$ from $R^{(l)}$ to $R^{(l+1)}$. Let $[\mathbf{u}_s], [\mathbf{u}_f]$ denote the jumps of the solid and fluid displacement vectors at $\Gamma^{(f,l)}$, *i.e.* $[\mathbf{u}_s] = \left(\mathbf{u}_s^{(l+1)} - \mathbf{u}_s^{(l)}\right)|_{\Gamma^{(f,l)}}$, where $\mathbf{u}_s^{(l)}$ denotes the displacement values in $R^{(l)}$. The following boundary conditions on $\Gamma^{(f,l)}$ are derived in Nakawa, S. and Schoenberg, M. A. (2007):

$$[\mathbf{u}_s \cdot \nu_{l,l+1}] = \eta_N \left((1-\alpha\tilde{B}(1-\Pi))\tau(\mathbf{u})\nu_{l,l+1}\cdot\nu_{l,l+1} - \alpha\frac{1}{2}\left((-p_f^{(l+1)}) + (-p_f^{(l)})\right)\Pi\right), \quad (5)$$

$$[\mathbf{u}_s \cdot \chi_{l,l+1}] = \eta_T\, \tau(\mathbf{u})\nu_{l.l+1}\cdot\chi_{l,l+1}, \quad (6)$$

$$[\mathbf{u}_f \cdot \nu_{l,l+1}] = \alpha\eta_N\left(-\tau(\mathbf{u})\nu_{l,l+1}\cdot\nu_{l,l+1} + \frac{1}{\widetilde{B}}\frac{1}{2}\left((-p_f^{(l+1)}) + (-p_f^{(l)})\right)\right)\Pi, \quad (7)$$

$$(-p_f^{(l+1)}) - (-p_f^{(l)}) = \frac{i\omega\mu\Pi}{\widehat{\kappa}}\frac{1}{2}\left(\mathbf{u}_f^{(l+1)} + \mathbf{u}_f^{(l)}\right)\cdot\nu_{l,l+1} \quad (8)$$

$$\tau(\mathbf{u})\nu_{l,l+1}\cdot\nu_{l,l+1} = \tau(\mathbf{u})\nu_{l+1,l}\cdot\nu_{l+1,l} \quad (9)$$

$$\tau(\mathbf{u})\nu_{l,l+1}\cdot\chi_{l,l+1} = \tau(\mathbf{u})\nu_{l+1,l}\cdot\chi_{l+1,l}. \quad (10)$$

Here $\eta_N$ and $\eta_T$ are the normal and tangential fracture compliances, respectively and $\widehat{\kappa} = \kappa/h$. The fracture dry plane wave modulus $H_m = K_m + (4/3)G$ and the dry fracture shear modulus $G$ are defined in terms of the fracture aperture $h$ and the fracture compliances as $\eta_N = \dfrac{h}{H_m}$, $\eta_T = \dfrac{h}{G}$.

Besides, $\Pi(\varepsilon) = \tanh\varepsilon/\varepsilon$, $\widetilde{B} = (\alpha M)/H_U$ and

$$\varepsilon = \frac{(1+i)}{2}\left(\frac{\omega\,\mu\,\alpha\,\eta_N}{2\widetilde{B}\widehat{\kappa}}\right)^{1/2}, \quad \alpha = 1 - K_m/K_s.$$

Following Gelinsky, S. and Shapiro, S. A. (1997) and Krzikalla, F. and Müller, T. (2011), an horizontally fractured Biot medium behaves as a TIV medium with vertical symmetry axis at long wavelengths. Denote by $\sigma_{ij}(\widetilde{\mathbf{u}}_s)$ and $\varepsilon_{ij}(\widetilde{\mathbf{u}}_s)$ the stress and strain tensor components of the equivalent TIV medium, where $\widetilde{\mathbf{u}}_s$ denotes the solid displacement at the macroscale. The stress-strain relations, stated in the space-frequency domain, are Carcione (2007)

$$\sigma_{11}(\widetilde{\mathbf{u}}_s) = p_{11}\,\varepsilon_{11}(\widetilde{\mathbf{u}}_s) + p_{12}\,\varepsilon_{22}(\widetilde{\mathbf{u}}_s) + p_{13}\,\varepsilon_{33}(\widetilde{\mathbf{u}}_s), \quad (11)$$

$$\sigma_{22}(\widetilde{\mathbf{u}}_s) = p_{12}\,\varepsilon_{11}(\widetilde{\mathbf{u}}_s) + p_{11}\,\varepsilon_{22}(\widetilde{\mathbf{u}}_s) + p_{13}\,\varepsilon_{33}(\widetilde{\mathbf{u}}_s), \quad (12)$$

$$\sigma_{33}(\widetilde{\mathbf{u}}_s) = p_{13}\,\varepsilon_{11}(\widetilde{\mathbf{u}}_s) + p_{13}\,\varepsilon_{22}(\widetilde{\mathbf{u}}_s) + p_{33}\,\varepsilon_{33}(\widetilde{\mathbf{u}}_s), \quad (13)$$

$$\sigma_{23}(\widetilde{\mathbf{u}}_s) = 2\,p_{55}\,\varepsilon_{23}(\widetilde{\mathbf{u}}_s), \quad (14)$$

$$\sigma_{13}(\widetilde{\mathbf{u}}_s) = 2\,p_{55}\,\varepsilon_{13}(\widetilde{\mathbf{u}}_s), \quad (15)$$

$$\sigma_{12}(\widetilde{\mathbf{u}}_s) = 2\,p_{66}\,\varepsilon_{12}(\widetilde{\mathbf{u}}_s). \quad (16)$$

To determine the coefficients in (11)-(16), we applied five compressibility and shear FE tests to representative 2D samples of fractured poroelastic materials. Each test consists on solving Biot' s equations (3) with the fracture boundary conditions (5)-(10) and additional boundary conditions representing compressibility tests in the parallel and normal directions to the fracture layering to determine $p_{11}$ and $p_{33}$, respectively, a test applying simultaneous compressions in both the normal and parallel directions to the fracture layering to determine $p_{13}$, and two shear tests to determine $p_{55}$ and $p_{66}$; a detailed description of the FE tests can be found in (Carcione, J. M. et al., 2011) and (Santos, J. E. et al., 2011).

## NUMERICAL EXAMPLES

The FE procedure was used to determine the complex stiffnesses $p_{IJ}(\omega)$, and the associated energy velocities and dissipation coefficients were computed as in Carcione (2007). In all the experiments we used square samples of side length 20 cm, with 9 equally spaced fractures of aperture $h$ = 2mm. The samples were discretized with a $100 \times 100$ uniform mesh. Both background and fractures have grain density $\rho_s = 2650$ kg/m$^3$ and bulk modulus $K_s = 37$ GPa.

The first experiment validate the FE procedure against the analytical solution given in Krzikalla, F. and Müller, T. (2011). The background has dry modulus $K_m$ = 11.7 GPa, shear modulus $G$ = 13.9 GPa, porosity $\phi = 0.25$ and permeability $\kappa$ = 0.246 D, while the corresponding values for the fractures are $K_m$ = 0.57 GPa, $G$ = 0.68 GPa, $\phi$= 0.5 and $\kappa$ = 4.4 D. In this example, we consider a brine saturated sample, with brine having density $\rho_f$ = 1040 kg/m$^3$, viscosity $\mu$ = 0.0018 Pa s and bulk modulus $K_f$= 2.25 GPa. Figures 1, 2, 3 and 4 show polar plots of the quality factors and energy velocity vectors for qP, qSV waves as functions of the propagation angle, and Figure 5 polar plots of the energy velocity vector for SH waves. Frequency is 5 MHz. Here 0 degrees and 90 degrees correspond to waves arriving parallel and normal to the fracture layering, respectively. A good agreement between the numerical and analytical curves is obtained for all angles. The qP curves show strong attenuation for waves arriving normal to the fracture layering. The qSV wave has no loss along the directions parallel and normal to the fracture layering, showing maximum attenuation at about 45 degrees. SH waves are lossless and show anisotropy velocity.

The second experiment considers the same sample for several percentages of patchy brine-$CO_2$ saturation, with brine having the same properties of the first example, while $CO_2$ has density 500 kg/m$^3$, viscosity 0.00002Pa·s and bulk modulus 0.025GPa. Patchy $CO_2$-brine distributions were generated using the von Karman self-similar correlation function (Frankel, A. and Clayton, R. W., 1986). The procedure to generate patchy saturation distributions is explained in Carcione, J. M. et al. (2011). Figure 6 displays a map of the patchy $CO_2$-brine fluid density distribution in the pore space for a 10 % $CO_2$ global saturation. Figures 7, 8, 9 and 10 show polar plots of quality factors and energy velocity vectors of qP, qSV waves as a function of the propagation angle for 0 %, 10 %, 50 % and 100 % global $CO_2$ saturations. Frequency is 5 MHz. Figure 7 shows that qP anisotropy is enhanced by patchy saturation, is maximum for qP waves arriving normally to the fracture layering, decreases as $CO_2$ saturation increases and vanishes at 100 % $CO_2$ saturation.

For qSV waves, Figure 8 shows that patchy saturation enhances qSV anisotropy, is strong for angles between 30 and 60 degrees and decreases as $CO_2$ saturation increases, vanishing at 100 %

$CO_2$ saturation.

Figures 9 and 10 display qP and qSV energy velocities, showing that patchy saturation has little effect on velocity anisotropy. Finally, SH waves show moderate velocity anisotropy, with values little affected by the presence of the $CO_2$ patches.

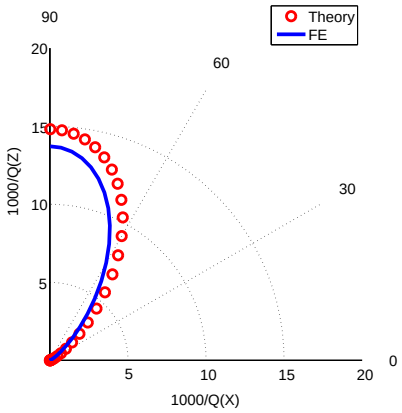


Figure 1: Dissipation factor of qP waves at 5MHz. The solid line indicate the numerical values.

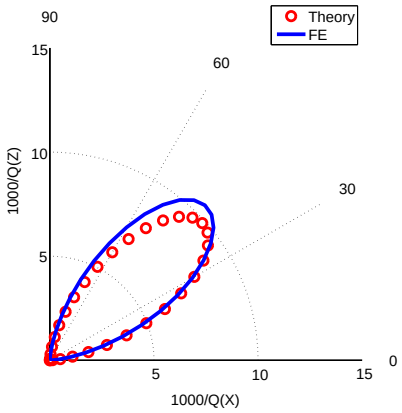


Figure 2: Dissipation factor of qSV waves at 5MHz. The solid line indicate the numerical values.

## CONCLUSIONS

This work presented a finitce element procedure to determine the five complex and frequency-dependent stiffnesses of the TIV medium equivalent to a horizontally fractured Biot medium, with fractures represented as internal boundary conditions. The methodology was first validated against a theory valid for homogeneous layers and fluid flow normal to the fracture layering. Then, the technique was applied for several percentages of patchy brine-$CO_2$ saturation, where was concluded that for qP and qSV waves patchy saturation affects more Q-anisotropy than velocity anisotropy, and SH velocity is almost unaffected by patchy saturation.

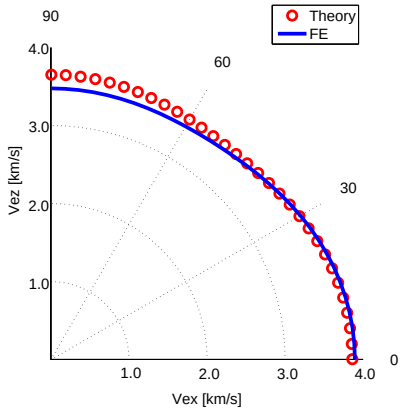


Figure 3: Polar representation of the qP energy velocity vector at 5MHz. The solid line indicate the numerical values.

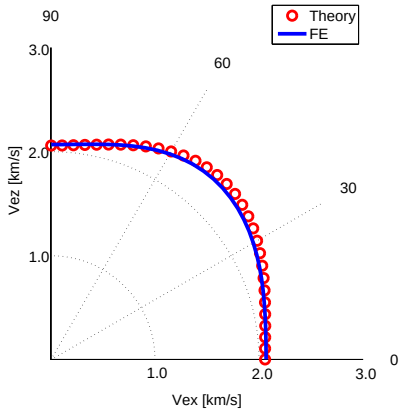


Figure 4: Polar representation of the qSV energy velocity vector at 5MHz. The solid line indicate the numerical values.

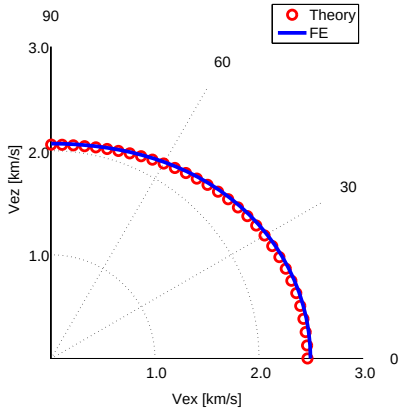


Figure 5: Polar representation of the SH energy velocity vector at 5MHz. The solid line indicate the numerical values.

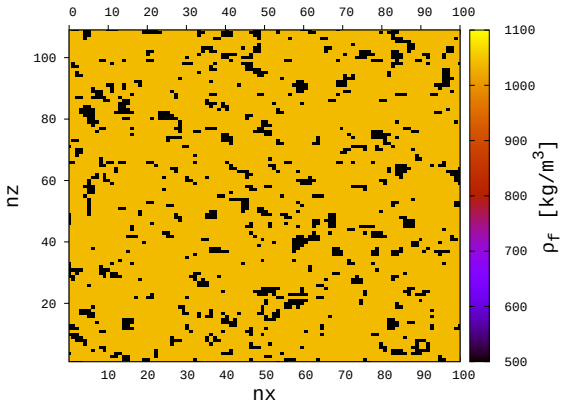


Figure 6: Fluid density distribution (kg/m$^3$) for 10 % patchy brine-$CO_2$ saturation. Black regions correspond to full $CO_2$ saturation.

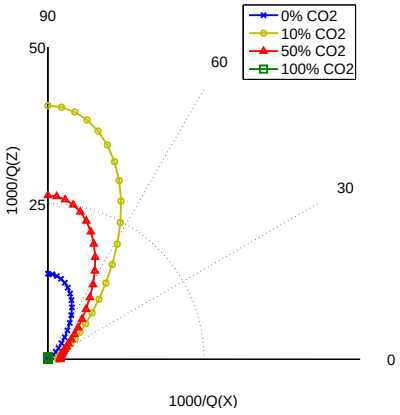


Figure 7: Dissipation factor of qP waves at 5MHz for the patchy saturation case.

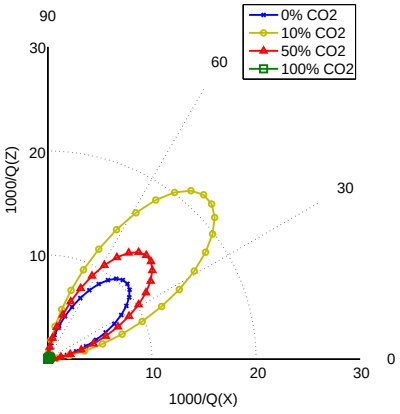


Figure 8: Dissipation factor of qSV waves at 5MHz for the patchy saturation case.

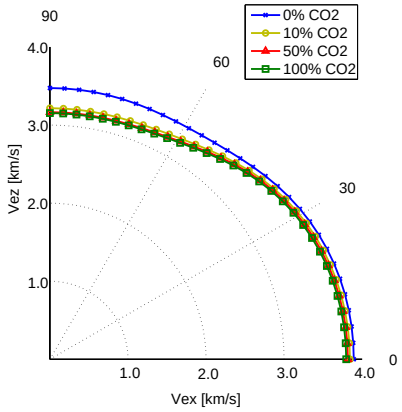


Figure 9: Polar representation of the qP energy velocity vector at 5MHz for the patchy saturation case.

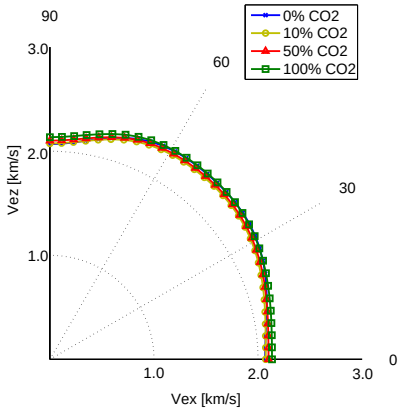


Figure 10: Polar representation of the qSV energy velocity vector at 5MHz for the patchy saturation case.

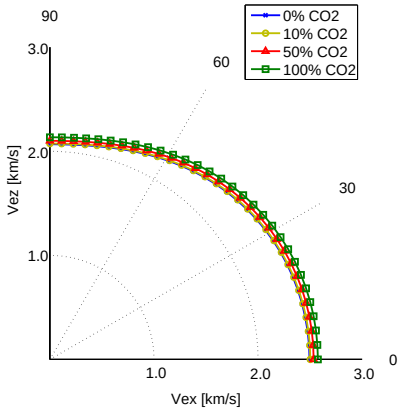


Figure 11: Polar representation of the SH energy velocity vector at 5MHz for the patchy saturation case.

## REFERENCES

Biot, M.A., 1962, Mechanics of deformation and acoustic propagation in porous media: Journal of Applied Physics, **33**, 1482–1498.

Carcione, J. M., 2007, Wave fields in real media: Wave Propagation in Anisotropic, Anelastic, Porous and Electromagnetic Media, Handbook of Geophysical Exploration, vol. 38: Elsevier (2nd edition, revised and extended).

Carcione, J. M., Santos, J. E., and Picotti, S., 2011, Anisotropic poroelasticity and wave-induced fluid flow. Harmonic finite-element simulations: Geophysics Journal International, **186**, 1245–1254.

Frankel, A. and Clayton, R. W., 1986, Finite difference simulation of seismic wave scattering: implications for the propagation of short period seismic waves in the crust and models of crustal heterogeneity: Journal of Geophysical Research, **91**, 6465–6489.

Gelinsky, S. and Shapiro, S. A., 1997, Poroelastic Backus-averaging for anisotropic, layered fluid and gas saturated sediments: Geophysics, **62**, 1867–1878.

Gurevich, B., 2003, Elastic properties of saturated porous rocks with aligned fractures: Journal of Applied Geophysics, **54**, 203–218.

Gurevich, B., Brajanovski, M., Galvin, R. J., Müller, T. M., and Toms-Stewart, J., 2009, P-wave dispersion and attenuation in fractured and porous reservoirs–poroelasticity approach: Geophysical Prospecting, **57**, 225–237.

Krzikalla, F. and Müller, T., 2011, Anisotropic P-SV-wave dispersion and attenuation due to interlayer flow in thinly layered porous rocks: Geophysics, **76**, WA135.

Nakawa, S. and Schoenberg, M. A., 2007, Poroelastic modeling of seismic boundary conditions across a fracture: Journal of the Acoustical Society of America, **122**, 831–847.

Santos, J. E., Carcione, J. M., and Picotti, S., 2011, Analysis of mesoscopic loss effects in anisotropic poroelastic media using harmonic finite element simulations: 81th Annual International Meeting, SEG, Expanded Abstracts, 2211–2215.